High-temperature stability of electron transport in semiconductors with strong spin-orbital interaction

G. Tomaka, J. Grendysa, P. Śliż, C. R. Becker,* J. Polit, R. Wojnarowska, A. Stadler,† and E. M. Sheregii‡
Centre for Microelectronics and Nanotechnology, University of Rzeszow Pigonia str. 1, 35-959 Rzeszow, Poland
(Received 10 September 2015; revised manuscript received 15 April 2016; published 11 May 2016)

Experimental results of the magnetotransport measurements (longitudinal magnetoresistance R_{xx} and the Hall resistance R_{xy}) are presented over a wide interval of temperatures for several samples of $Hg_{1-x}Cd_xTe$ ($x \approx 0.13$–0.15) grown by MBE—thin layers (thickness about 100 nm) strained and not strained and thick ones with thickness about 1 μm. An amazing temperature stability of the SdH-oscillation period and amplitude is observed in the entire temperature interval of measurements up to 50 K. Moreover, the quantum Hall effect (QHE) behavior of the Hall resistance is registered in the same temperature interval. These peculiarities of the R_{xx} and R_{xy} for strained thin layers are interpreted using quantum Hall conductivity (QHC) on topologically protected surface states (TPSS) [C. Brüne *et al.*, Phys. Rev. Lett. **106**, 126803 (2011)]. In the case of not strained layers it is assumed that the QHC on the TPSS (or on the resonant interface states) contributes also to the conductance of the bulk samples.

DOI: 10.1103/PhysRevB.93.205419

I. INTRODUCTION

One of the obvious properties of semiconductors is their strong dependence on external conditions such as temperature, illumination, or pressure. Topological insulators (TI), discovered during the last decade, have augmented our knowledge on this matter. TI is a new class of quantum matter with conducting surface states, topologically protected against time-reversal-invariant perturbations and an insulating bulk. The physics of TI links the structures of d dimensions with their boundaries in $d-1$ dimensions: A TI is a state of quantum matter that behaves as an insulator in its interior and as a metal on its boundaries [1].

The first topological insulators which were observed via the quantum spin Hall effect concern a two-dimension electron gas (2DEG) with a spin structure on a 1D edge. They were discussed theoretically [2,3], predicted to occur in HgTe quantum wells [4], and then experimentally verified by König *et al.* [5]. Thereafter Liang Fu *et al.* [6] proposed the 3D version of topological insulators, predicted to occur in Bi-Sb alloys by Fu and Kane [7], and experimentally detected with angle-resolved photoemission spectroscopy ARPES by Hsieh *et al.* [8].

Subsequently, the quantum Hall effect (QHE) in the surface layer with topologically protected surface states (TPSS) was observed via transport experiments in strained bulk mercury telluride (HgTe) [9]. As predicted by B. A. Bernevig, T. L. Hughes, and S.-C. Zhang [4], TPSS occur at the surface of HgTe as massless Dirac points (Dirac cones with a linear dependence of the electron energy on momentum in terms of the band structure) because of the Γ_6 and Γ_8 band crossing. Generally, it is caused by strong spin-orbital interaction in these materials which lifts the Γ_8 band above the Γ_6 band in the bulk part of the sample [10].

This kind of TPSS is characterized by a Z_2 topological invariant, requiring gapless electronic states to exist on the boundary of the sample, which is a strong topological insulator and is robust in the presence of disorder [4,11,12]. Such strong topological insulators have surface states, with the Fermi surface enclosing an odd number of Dirac points and being associated with the Berry phase of Ref. [13]. This defines a topological metal surface phase, which is predicted to have novel electronic properties [14–16]. There is some similarity with the half-Heusler alloys. For example, PtMnBi show semimetallic properties in the α phase, and the effects of the spin-orbit interaction shifts of the valence bands and the indirect semiconducting gap with respect to the spin polarized results [17,18].

Also BiSb alloys, Bi_2Se_3, Bi_2Te_3, and Sb_2Te_3 crystals show the 3D TI properties [19–23]. The next class of bulk topological insulators discovered during the last decade includes $TlSbSe_2$, $TlSbTe_2$, $TlBiSe_2$, and $TlBiTe_2$ [24,25], as well as septuple-layer topological insulators [24]. Recently, well-developed TPSS were reported to occur in the QHE of $BiSbTeSe_2$, an intrinsic TI bulk material, 120 and 160 nm thick [26]. In addition, the dominate contribution of the surface metallic conductivity in the total sample resistance of BiSbTeSe above 120 K, was noticed. Thus, a new feature of the electron transport properties of semiconductors with strong spin-orbital interaction could take place: the surface metallic conductance. The same, as will be shown below, can be said of mercury cadmium telluride solid solutions—arguably the best material for infrared devices [27]. The QHE according to Brüne *et al.* [9] (similar results were presented later in Ref. [28]) was displayed for comparably thin (70 nm) strained samples. It is interesting to check the same experiment for thin strained layers of semimetal alloys of HgCdTe as well as for no strained layers of these alloys.

The paper describes experimental results obtained for bulk $Hg_{1-x}Cd_xTe$ samples with $x \approx 0.13$–0.16 corresponding to a semimetallic type of band structure, i.e., the Γ_8 band is higher than Γ_6. However it is close to the critical point at which the Γ_6 and Γ_8 bands cross, that should occur in the temperature region from 0.4 to 150 K depending on the x value [27]. Section II

*Physics Department, University of Illinois at Chicago, Chicago, Illinois, USA.
†Rzeszow University of Technology.
‡Corresponding author: sheregii@ur.edu.pl

presents the experimental details: the samples grown by MBE technology, the magnetotransport experiment procedure, and experimental data including the SdH-oscillations, the QHE behavior of the Hall resistance observed in a wide temperature region for the samples with different levels of doping including comparably thick layers. In Sec. III we discuss the origin of the quantum Hall conductance behavior of the Hall resistance for thin strained layers, thin not strained layers, and comparatively thick ones. Finally, in Sec. IV we summarize our findings and draw conclusions.

II. EXPERIMENT

A. Samples

The $Hg_{1-x}Cd_xTe$ samples were grown in a Riber Compact 21 molecular beam epitaxial (MBE) system. The CdTe and Te fluxes were chosen and subsequently adjusted in order to grow the $Hg_{1-x}Cd_xTe$ layers with a zero gap at approximately 4–50 K. Two types of substrates were used to perform the experiment: (i) (001) oriented GaAs substrates were applied with the MBE grown CdTe buffer that produced ∼0.3% mismatch with the next thin MBE grown $Hg_{1-x}Cd_xTe$ layer; (ii) (112)*B* orientated CdZnTe substrates were employed and the $Hg_{1-x}Cd_xTe$ was grown directly on the CdZnTe(112)*B* substrate surface which have a lattice constant practically (with an uncertainty of 0.01%) equal to that of bulk $Hg_{1-x}Cd_xTe$ ($x \approx 0.13$). Consequently, three types of sample were grown and measured, namely: type A—$Hg_{1-x}Cd_xTe$ thin strained layers on the GaAs/CdTe substrates (about 100 nm thick); type AB—$Hg_{1-x}Cd_xTe$ thin not strained layers on the CdZnTe(112)*B* substrates (about 100 nm thick); type B—$Hg_{1-x}Cd_xTe$ thick not strained layers on the CdZnTe(112)*B* substrates (samples B4 and B6–B9 are about 1 μm thick; the sample B5 is above 2 μm thick). The $Hg_{1-x}Cd_xTe$ layers were substantially doped with iodine by means of a CdI_2 effusion cell for samples A9, AB9, B8, and B9 and by means of an In effusion cell for samples A4, AB4, B4, B5, and B6. SIMS measurements and the reflection maxima of E_1 and $E_1+\Delta_1$ in the region of fundamental absorption of the $Hg_{1-x}Cd_xTe$ alloys [29] were used to confirm the composition, level of doping and thickness of the grown layers (see Table I).

Parameters of the resulting layers are shown in Table I. Fifteen samples with different compositions ($x = 0.13$–0.16), thicknesses and levels of doping, were investigated.

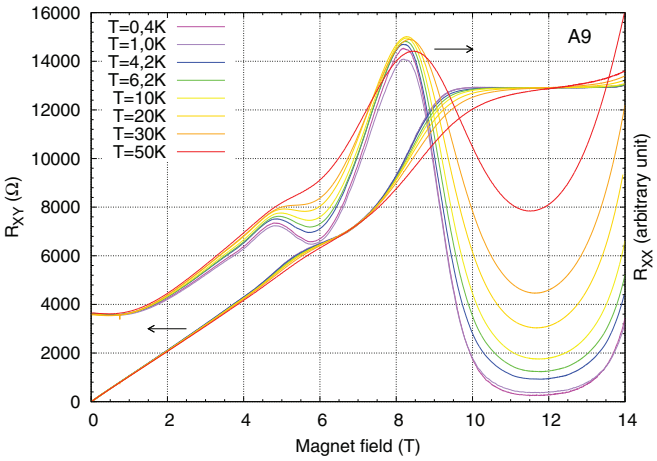

FIG. 1. Magnetoresistances R_{xx} and R_{xy} vs magnetic field in the temperature region of 0.4–50 K for sample A9. Three plateaus are seen on the R_{xy} curves; the resistances in these plateaus in the temperature region of 0.4–20 K is equal to values $h/\nu e^2$ when $\nu = 2$, 4, and 6.

B. Magnetotransport measurements

The magnetotransport measurements were performed using a cryomagnet system from ICEoxford, which is capable of voltage measurements in the temperature region from 0.25 to 290 K in magnetic fields up to 14 T. The direction of the magnetic field B was perpendicular to the plane of the investigated layer in the samples. Four-terminal longitudinal (R_{xx}) and Hall (R_{xy}) resistances were measured with standard lock-in techniques at a low frequency (<20 Hz) and with an excitation current of 0.5–1.0 μA. Four measurements were made, i.e., for the two directions of the magnetic field and for increasing and decreasing magnetic fields, with the subsequent averaging of each measurement of the longitudinal magnetoresistance and Hall resistance at a given temperature.

C. Results

The results of the magnetotransport measurements obtained for sample A9—strained thin layer on the GaAs/CdTe substrate—are presented in Fig. 1. The $R_{xx}(B)$ and $R_{xy}(B)$ curves are shown for different temperatures over a wide range from 0.4 K to 50 K. The well-defined quantized plateaus in

TABLE I. Parameters of the samples grown by MBE.

Nr	Composition x, mol.	Substrate	Thickness, nm	Level of the iodine bulk doping 10^{17} cm^{-3}	Level of the indium bulk doping 10^{17} cm^{-3}
A4	0.155	GaAs/CdTe(001)	100		0.5
A9	0.135	GaAs/CdTe(001)	100	5.0	
AB4	0.155	CdZnTe(112)*B*	100		0.5
AB9	0.135	CdZnTe(112)*B*	100	5.0	
B4	0.155	CdZnTe(112)*B*	840		0.5
B5	0.135	CdZnTe(112)*B*	2480		0.8
B6	0.150	CdZnTe(112)*B*	1280		3.0
B8	0.145	CdZnTe(112)*B*	950	0.5	
B9	0.135	CdZnTe(112)*B*	1100	5.0	

R_{xy} with values $h/(2e^2) = 12.9\,\mathrm{k}\Omega$ accompanied by vanishing R_{xx} is observed at 0.4 K.

It is seen by pronounced plateaus in R_{xy} at values equal to about 6.5 kΩ as well as one less clear at about 4.3 kΩ. The $R_{xx}(B)$ curves exhibit pronounced SdH oscillations whose positions of maxima strongly corresponds to stairs before plateaus on the $R_{xy}(B)$ curve. Described particularities on the $R_{xx}(B)$ and $R_{xy}(B)$ curves of sample A9 explicitly indicate on the integer quantum Hall effect (IQHE) and Shubnikov-de Haas (SdH) oscillations characteristic for 2D electron gas. The quantization in integer multiples of $\sigma_0 = e^2/h$ is evident with the Landau filling factor ν equals to 2, 4, and 6. It is necessary to underline that the $R_{xx}(B)$ and $R_{xy}(B)$ curves are reproducible up to 20 K and above this temperature the integer quantum Hall conductivity (IQHC) is observed up to 50 K.

The same magnetotransport measurements are repeated for sample AB9—no strained thin layer on the CdZnTe(112)B substrate. The remarkable temperature stability of the $R_{xx}(B)$ and $R_{xy}(B)$ curves characteristic for sample A9 is repeated for sample AB9 [see Fig. 2(a)]. Similarly, one can see the plateaulike features of the R_{xy} curve and corresponding SdH maxima on the R_{xx}(B) curve, but the quantization in integer multiples of $\sigma_0 = e^2/h$ is not evident. The latter can be attributed to the availability of a parallel conductance channel from the sample interior that decreases the values of the R_{xy} resistance in the plateaus [26,30]. In order to more quantitatively estimate the surface contribution to the total conductance, we fit our data to a simple model used in Refs. [31,32], where the total conductance is the parallel sum of the bulk conductance of $Hg_{1-x}Cd_xTe$ ($x = 0.13$) and the 2D surface conductance. According to this scheme, the values of R_{xy} for the plateaus of QHE decrease proportionally due to the contribution of the bulk part of the sample. The calculation of the R_{xy} resistance (for the whole sample) assumed that the QHE values $R_{xx} = h/\nu e^2$ of the voltage are generated in the surface sheet, and the classic Hall effect occurs in the bulk part of the sample. The results of calculation and experimental data obtained for the sample AB9 are compared in Fig. 2(b). It can be seen that the results of simulation approximate very well the observed plateaus in the case of odd values of the filling factor: $\nu = 3, 5, 7$. Similar experimental data take place for sample AB4 also thin layer of semimetal $Hg_{1-x}Cd_xTe$ ($x = 0.155$) grown on the CdZnTe(112)B substrate.

Figures 3 and 4 show the measurements for four samples from those listed in Table I: B4, B5, B6, and B9 which are thick not strained layers. The $R_{xx}(B)$ and $R_{xy}(B)$ curves recorded for sample B9 are shown in Fig. 3(a) for different temperatures over a wide range from 0.4 to 50 K. It comes to our attention that the results are reproducible at different temperatures up to 50 K; that seems unexpected for this thick sample (about 1 μm, see Table I). Temperature increase beyond 50 K makes the plateaus less pronounced. The amazing temperature stability also concerns the positions of the observed SdH-oscillation maxima. These positions are reproducible up to 45 K and the amplitude of the SdH-maxima decreases slowly with increasing temperature above 50 K. The plateaulike features in R_{xy} in Figs. 3(a) and 4 are reminiscent of the IQHE, but in the present case the values of the R_{xy} resistance in the plateaus for sample B9 are low, of the

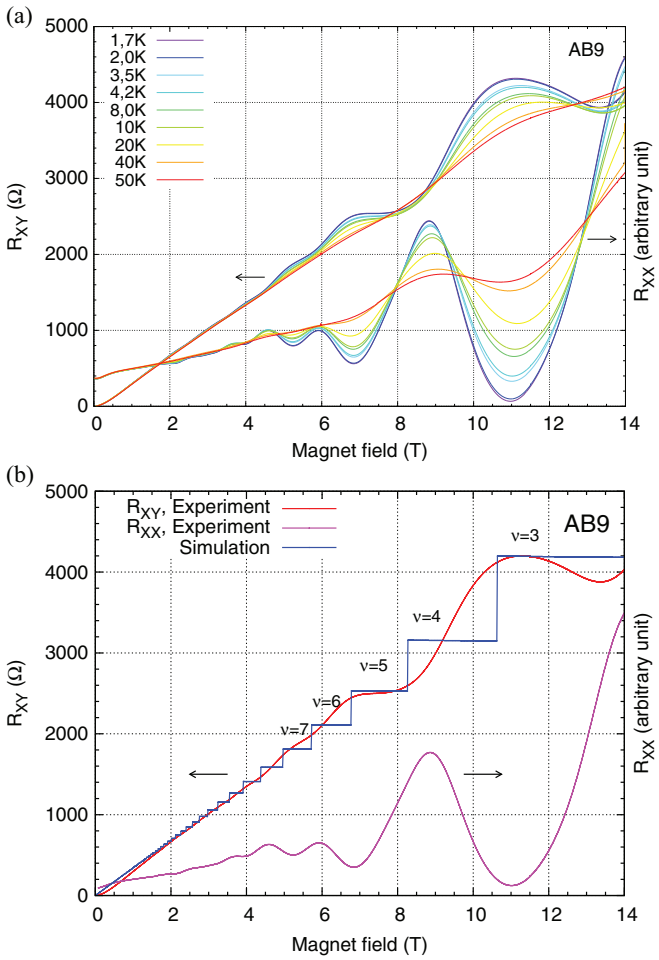

FIG. 2. (a) Magnetoresistances R_{xx} and R_{xy} vs magnetic field in the temperature region of 0.4–50 K for sample AB9; (b) Calculations (blue line) of the R_{xy} resistance for the entire sample AB9 at 1.7 K performed according to a scheme of taking the parallel sum of the QHE values of the voltage generated in the surface sheet and a classic Hall voltage in the bulk part of sample AB9. It can be seen that the odd values of filling factor $\nu = 3, 5, 7$, and 9 correspond to experimentally observed plateaus at temperature 1.7 K.

order of 10–20 Ω. On the other hand, in the case of sample B9 the ratio $R_{xy}^{III}(B)/R_{xy}^{V}(B) = 20.0\ \Omega/13.0\ \Omega = 1/3 : 1/5$ and $R_{xy}^{V}(B)/R_{xy}^{VII}(B) = 13.0\ \Omega/11.0\ \Omega = 1/5 : 1/7$ where $R_{xy}^{III}(B)$ is the value of resistance in the plateaus at 11.0–14.0 T, $R_{xy}^{V}(B)$ is the value of resistance in the plateaus at 7.0–8.5 T, and $R_{xy}^{VII}(B)$ is the resistance at 5.5–6.5 T. Thus, these values of the resistance correspond to the magnitude for corresponding values of the filling factor of $\nu = 3$, 5, and 7, but they are smaller due to the parallel resistance in the sample. Similarly to the sample AB9, the calculation of the R_{xy} resistance (for the whole sample) assumed that the QHE values $R_{xy} = h/\nu e^2$ (ν is an integer) of the voltage are generated in the surface sheet, and the classic Hall effect occurs in the bulk part of the sample. The results of the calculation are compared with the experimental curve for sample B9 in Fig. 3(b). It can be seen that the results of the simulation approximate satisfactorily the observed plateaus in the case of odd values of the filling factor: $\nu = 3, 5, 7$.

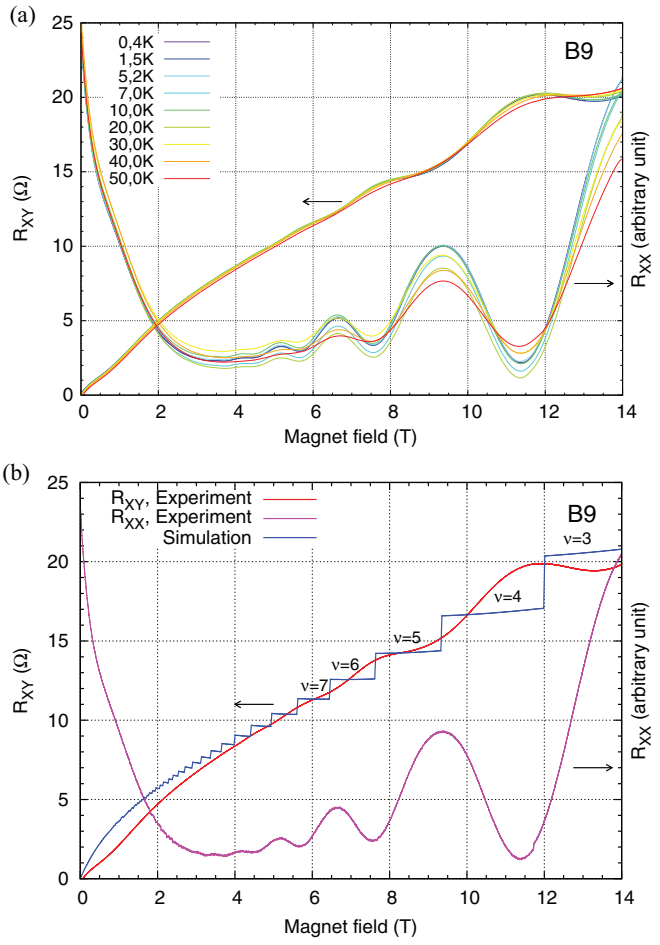

FIG. 3. (a) Magnetoresistances R_{xx} and R_{xy} vs magnetic field in the temperature region of 0.4–50 K for sample B9; (b) Calculations (blue line) of the R_{xy} resistance for the entire sample B9 at 4.2 K performed according to the same scheme as for sample AB9. It can be seen that the odd values of filling factor $\nu = 3, 5$, and 7 correspond to experimentally observed plateaus.

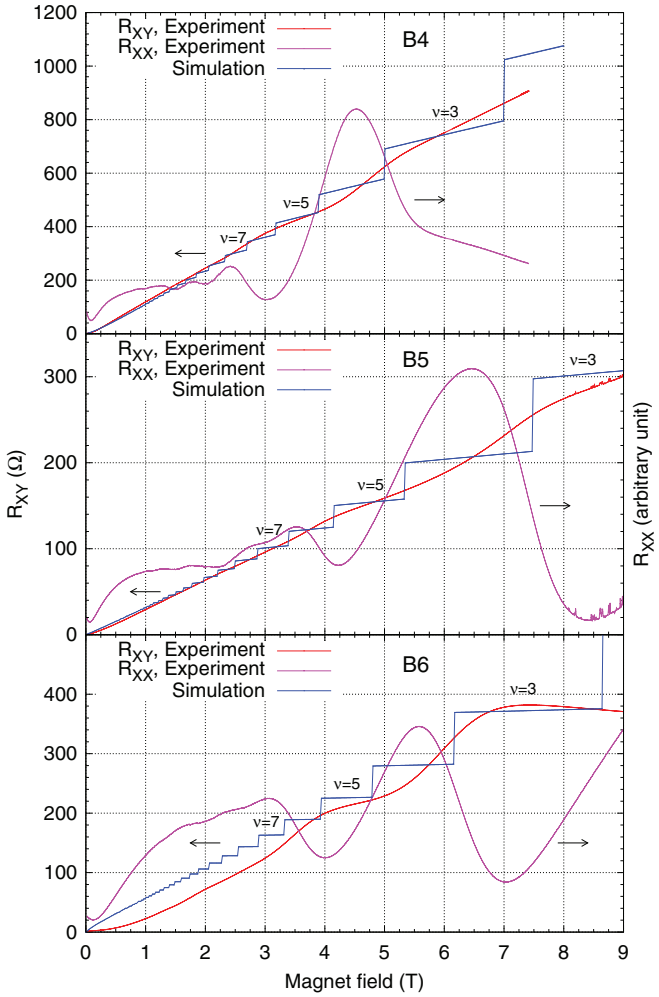

FIG. 4. Magnetoresistances R_{xx} and R_{xy} vs magnetic field in the temperature region of 0.4–2.3 K for samples B4, B5, and B6.

Similar curves were obtained for all samples of the B series. The results of the magnetotransport measurements obtained for samples B4, B5, and B6 are shown in Fig. 4 at approximately the same temperature (within an interval of 0.42–2.25 K). They exhibit the QHE behavior similar to that observed for the sample B9, even though the plateaus values of the resistance are different due to their dependence on the resistance of the bulk part of the samples.

Moreover, the proportions between values of the R_{xy} resistance corresponding to odd values of the ν factor in different plateaus are retained. For sample B5 the plateaus in the $R_{xy}(B)$ curve are less distinct. The results of calculating the $R_{xy}(B)$ resistance obtained in a similar way as for the samples AB9 and B9, are shown in Fig. 4 also. The stability of the R_{xy} and R_{xx} curves for samples B4 and B6 in the temperature interval of 0.4–45 K is similar to that of the sample B9. Other temperature behavior is observed for sample B5: The plateaus and SdH oscillations disappeared after reaching 30 K. It is interesting to note that in the case of 2DEG in the HgCdTe/HgTe/HgCdTe quantum well the resistance at the charge neutrality point was found to be temperature independent at low temperatures [33].

III. INTERPRETATION

A. General consideration

The model proposed for bulk HgTe [9] seems the most appropriate tool to explain the above results of magnetotransport measurements made for the $Hg_{1-x}Cd_xTe$ strained layer A9 (similar ones are for A4). The TPSS exist at the border of the sample surface layer with air as well as at the border with the substrate whose 2D layers with Dirac fermions contribute to the electron transport of the whole sample with the energy gap in the interior.

Based on the studies made by cited above authors [9,26,30] and considering earlier works [34,35], we can understand the observed IQHC as the sum of a half integer QHC from the top surface and another half integer QHC from the bottom surface. In other words, the IQHC is quantized according to

$$\sigma_{xy}^{\text{total}} = \nu\frac{e^2}{h} = \sigma_{xy}^{\text{top}} + \sigma_{xy}^{\text{bottom}} = (\nu_t + \nu_b)\frac{e^2}{h}$$
$$= (N_t + N_b + 1)\frac{e^2}{h} \quad (1)$$

with top (bottom) surface QHC

$$\sigma_{xy}^{\text{top(bottom)}} = \nu_{t(b)}\frac{e^2}{h} = \left(N_{t(b)} + \frac{1}{2}\right)\frac{e^2}{h} \quad (2)$$

where $\nu_{t(b)}$ and $N_{t(b)}$ are the Landau filling factor and Landau level index of top (bottom) surface corresponding to the QH state.

When top and bottom surface have the same filling factor, and both surfaces have the same density, i.e. $N_t = N_b$, then the resulting expression for the QHC, according to (1), is as follows:

$$\sigma_{xy} = (2N + 1)\frac{e^2}{h}. \quad (3)$$

Hence, the filling factor ν can only have odd values. In case of asymmetric conductivity along top and the bottom surface the expression (1) should be applied and the filling factor ν can be even or half-integer value if the conductivity along the bottom surface disappeared.

B. Samples of A series

The strong TI exists in the case of the sample A9: The energy gap of about 10 meV is formed in the sample interior due to the tension, and the TPSS are on surfaces due to crossing of the Γ_8 and Γ_6 bands, similarly to HgTe strained layer [9]. On the other hand, we should assume that the conditions of electron transport are different on the top and bottom surfaces because the first one is practically ideal (according to the AFM picture), but the bottom surface could be in a different situation at the interface with the CdTe buffer layer due to mismatch. It means that the asymmetric conductivity along the top and bottom surfaces could be produced by latter fact, namely—different density of the fermions.

As was shown in Sec. II the $R_{xy}(B)$ curves demonstrate the QHE with the Landau filling factor ν equals to 2, 4, and 6 in the case of sample A9. So, the filling factor is even, and, according to the expression (1) the next the situation may be realized, for example: in case of $\nu = 2 - N_t = 0$ and $N_b = 1$, for $\nu = 4 - N_t = 1$ and $N_b = 2$ and for $\nu = 6 - N_t = 2$ and $N_b = 3$.

C. Samples of AB series

The sample AB9 was obtained by MBE growth on the CdZnTe(112)B substrate with practically ideal match. Thus, there are no strains, and there is no origin of the energy gap in the sample interior. On the other hand, it is difficult to refute that in semimetallic $Hg_{1-x}Cd_xTe$ ($x < 0.16$), between the nominally designated conduction and valence bands, a small gap can occur due to various reasons (finally, this gap may be generated by a magnetic field). So, it is possible to assume that TPSS can exist in the case of samples AB9 and AB4 on the background of a small energy gap or on the background of the heavy hole states [36,37] (without a gap between the $\Gamma_8^{1/2}$ and $\Gamma_8^{3/2}$ states, which could be named as some resonance interface state, see more discussions below). This makes possible the same density of the Dirac fermions on top and bottom surfaces. In this case the IQHC according to Eq. (3) could be realized with odd values of the filling factor ν, but the parallel classic Hall effect takes place in the interior of the sample without an energy gap. This assuming is confirmed by Fig. 2(b) where the simulation curve approximates very well the observed plateaus on the R_{xy} experimental curve for sample AB9 and odd values of the filling factor: $\nu = 3$, 5, 7. High temperature stability of observed plateaus visible on the R_{xy} curves and of the SdH oscillations on the R_{xx} curves can be explained by this assuming the electron transport on the TPSS [or on the resonance interface state [36,37] (RIS)] dominates the electron transport in the whole sample AB9. This assuming concerns the sample AB4 also.

If the model of the electron transport applied to the sample AB9 is adequate, it becomes important to determine the thickness of a layer in which transport of Dirac fermions dominates. The experimental data obtained for the samples of B series could give an answer to this question.

D. Samples of B series

It is appropriate to start with the sample B9 which can be considered as a thicker version (1100 nm thick) of the sample AB9. As was shown in Sec. II, for the sample B9, the plateaus at 11.0–14.0 T corresponds to $\nu = 3$ and next one at 7.0–8.5 T − to $\nu = 5$, and another one at 5.5–6.5 T − to $\nu = 7$ [see Fig. 3(b)]. Thus, the odd integer IQHC is observed as it has been described for the sample AB9, but the plateaus resistances are considerably less because of the substantial contribution from the classical Hall effect in the sample bulk. High temperature stability of plateaus on the R_{xy} curves, as well as of the SdH oscillations on the R_{xx} curves shown in Fig. 3(a) in a wide temperature range, allows advancing the hypothesis concerning a major role which the electron transport on the RIS (or on the TPSS) plays in the electron transport within the whole sample B9 as well.

As to the samples B4 and B6, it should be noted that experimental data confirms the hypothesis given above. The only exception is the sample B5 with the thickness of 2840 nm (Table I).

IV. DISCUSSION AND SUMMARY

The above mentioned interpretation of the experimental results concerning the Landau level structure of a Dirac system can be confirmed by plotting the Landau level index as a function of 1/B [9,30,35]. That concerns mostly the samples of the series AB and B. Figure 5 is created through taking the magnetic field values corresponding to the Hall plateaus with $\nu = 9$, 7, 5, 3 from the R_{xy} curve in Figs. 2(b), 3(b), and 4 to plot the resulting N as a function of 1/B according to Eq. (3). The intercept of these plots for infinite magnetic field gives in the case of samples AB9, B9, B4, and B6 a value of $-1/2$, that provides additional evidence for describing the observed IQHC by the two Dirac cones model. For the sample B5 the intercept gives a 0 value that means the peculiarities visible on the R_{xx} curves can be attributed rather to the bulk part of the sample.

It is an unexpected result that the 2D-TPSS conductance (in the case of thick samples B9, B4, and B6 we prefer to call: the electron transport on the RSI) contributes to the total conductance in these slab-shaped samples with parallel top and

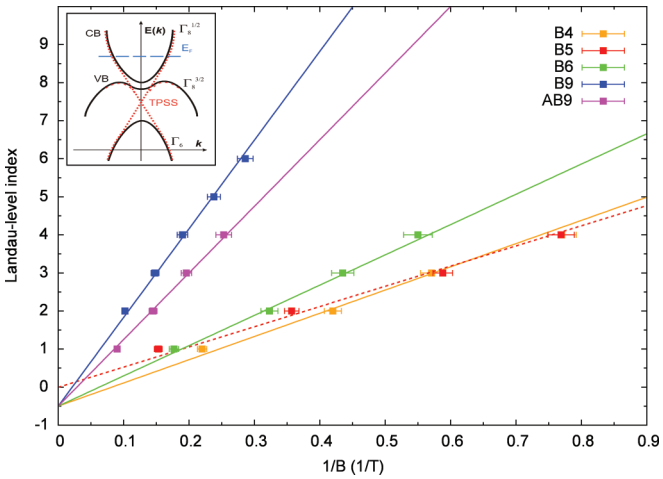

FIG. 5. Landau level index for the data of Figs. 2(b), 3(b), and 4 plotted as a function of inverse magnetic field. The intercept of this plot for infinite magnetic field gives a value of $-1/2$ for samples AB9, B9, B4, and B6, which provides evidence that the observed IQHC can be well described by the two Dirac cones model. In the case of the B5 sample a spin-splitted maxima of the SdH-oscillations are visible, and the positions corresponding to the $-N$ Landau index are plotted at what gives intercept "0." In the inset, the proposed energy-band structure with TPSS is shown.

bottom surfaces which surround (together with the side walls) a thick (about 1 μm) semimetal bulk component (topologically it is the same as a sphere). Surprisingly the Dirac point in the surface layer can exist in conjunction with the (heavy hole) band in the bulk part of the sample (see inset in Fig. 5) without an energy gap (in the case of samples of series AB and B) which usually takes place in TI. As was shown in Ref. [36], such TPSS states, designated as interface states, can couple to a heavy hole state and thus could be modified. Jie Ren *et al.* [37]: The topological phase transition from bulk CdTe to HgTe upon alloying and the massless Dirac-Kane semimetal phase at the critical composition ($x < 0.16$) are illustrated by computations based on a mixed-pseudo-potential simulation confirmed by the ARPES experiment: a topological surface state (TSS) band connecting from the Γ_6 band to the upper Γ_8 band (above the Fermi level) takes place.

An alternative interpretation of above presented results on the AB and B series samples could be the possibility of a surface layer at interface layer-air produced due to increase of the mercury content at the surface of the layer. That could form a narrow quantum well with 2DEG at the interface which could generate observed IQHC. The probability of that is negligible due to whatever any increase in the Hg content at surface was registered by SIMS in samples investigated. On the other hand, if such a quantum well could exist at the surface, the QHE would show all integer values of the Landau filling factor not only odd values and the intercept of the resulting N plotting

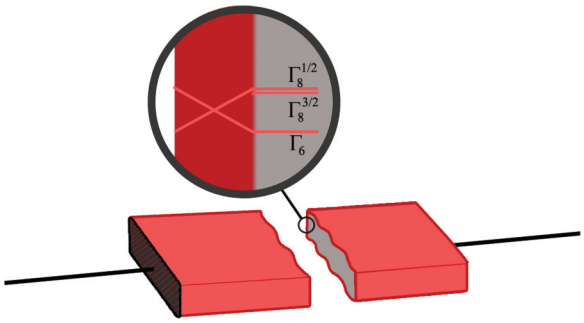

FIG. 6. Proposed conception of the electron transport in the semimetal bulk $Hg_{1-x}Cd_xTe$: The 2D-TPSS on parallel top and bottom surfaces (as well as on the side walls) form the metallic Berry phase (red color) surround the bulk semimetal part (gray color). As a result, metallic conductance on surfaces dominates the conductance of the entire sample.

as function of the 1/B would give value 0 not $-1/2$ as it takes place for samples AB9, B9, B4, and B6 (see Fig. 5).

Another interesting feature is that the observed IQHC is more pronounced in samples B6 and B9 which have higher electron densities. Specific screening properties of Dirac systems [38–40] can originate this phenomenon.

In summary, a quantized Hall conductance in the 3D $Hg_{1-x}Cd_xTe$ samples ($x < 0.16$) with thickness from 100 to 1280 nm and with different levels of n type doping, using either iodine or indium as dopants, is observed over a wide temperature region from 0.4 to 50 K. The experimental results lead to the hypothesis that quantum Hall conductance on the 2D-TPSS (or on the RSI) contributes to conductance of entire samples. A simple model with two Dirac cones satisfactorily explains the most salient features of the transport measurement of MBE grown and comparatively thick samples (up to 1280 nm) of semimetal $Hg_{1-x}Cd_xTe$. In other words, the conductance due to the TPSS (or RIS) at the interfaces of the approximately 3 nm thick lower layers with the semimetal bulk part of the investigated sample with thickness from 100 to 1280 nm, can dominate the conductance of the entire sample (see Fig. 6). It is a conception of the electron transport in the semimetal bulk $Hg_{1-x}Cd_xTe$ that could require a reinterpretation of previous experimental results on semimetal $Hg_{1-x}Cd_xTe$ layers (with thickness less as 1300 nm) which have been obtained over the last 40 years.

ACKNOWLEDGMENTS

We acknowledge support from the authorities of the Podkarpackie Voiwodership (Marshals Office of the Podkarpackie Voivodship of Poland), contract WND-PPK.01.03.00-18-053/12. We acknowledge also E. Bobko for performed lithography for samples investigated as well as M. Trzyna for the SIMS measurements and Prof. I. Izhnin, Prof. T. Wojtowicz, and Prof. J. Wrobel for valuable discussions.

[1] Shun-Qing Shen, *Topological Insulators. Dirac Equation in Condensed Matter*, Springer Series in Solid State Science 174 (Springer, Heidelberg, 2013).

[2] C. L. Kane and E. J. Mele, Phys. Rev. Lett. **95**, 226801 (2005).

[3] B. A. Bernevig and S.-C. Zhang, Phys. Rev. Lett. **96**, 106802 (2006).

[4] B. A. Bernevig, T. L. Hughes, and S.-C. Zhang, Science **314**, 1757 (2006).

[5] M. König, S. Wiedmann, C. Brüne, A. Roth, H. Buhmann, L. W. Molenkamp, Xiao-Lian Qi, and S.-C. Zhang, Science **318**, 766 (2007).

[6] Liang Fu, C. L. Kane, and E. J. Mele, Phys. Rev. Lett. **98**, 106803 (2007).

[7] Liang Fu and C. L. Kane, Phys. Rev. B **76**, 045302 (2007).

[8] D. Hsieh, D. Qian, L. Wray, Y. Xia, Y. S. Hor, R. J. Cava, and M. Z. Hasan, Nature (London) **452**, 970 (2008).

[9] C. Brüne, C. X. Liu, E. G. Novik, E. M. Hankiewicz, H. Buhmann, Y. L. Chen, X. L. Qi, Z. X. Shen, S.-C. Zhang, and L. W. Molenkamp, Phys. Rev. Lett. **106**, 126803 (2011).

[10] A. Delin and T. Klüner, Phys. Rev. B **66**, 035117 (2002).

[11] M. Z. Hasan and C. L. Kane, Rev. Mod. Phys. **82**, 3045 (2010).

[12] Xiao-Liang Qi and Shou-Cheng Zhang, Rev. Mod. Phys. **83**, 1057 (2011).

[13] M. Berry, Nat. Phys. **6**, 148 (2010).

[14] J. E. Moore and L. Balents, Phys. Rev. B **75**, 121306(R) (2007).

[15] Jeffrey C. Y. Teo, Liang Fu, and C. L. Kane, Phys. Rev. B **78**, 045426 (2008).

[16] Liang Fu and C. L. Kane, Phys. Rev. Lett. **100**, 096407 (2008).

[17] I. Galanakis, P. H. Dederichs, and N. Papanikolaou, Phys. Rev. B **66**, 174429 (2002).

[18] Wenjie Xie, Anke Weidenkaff, Xinfeng Tang, Qingjie Zhang, Joseph Poon, and Terry M. Tritt, Nanomaterials **2**, 379 (2012).

[19] Y. Xia, D. Qian, D. Hsieh, L. Wray, A. Pal, H. Lin, A. Bansil, D. Grauer, Y. S. Hor, R. J. Cava, and M. Z. Hasan, Nat. Phys. **5**, 398 (2009).

[20] H. Zhang, C.-X. Liu, X.-L. Qi, X. Dai, Z. Fang, and S.-C. Zhang, Nat. Phys. **5**, 438 (2009).

[21] Y. L. Chen, J. G. Analytis, J. H. Chu, Z. K. Liu, S. K. Mo, X. L. Qi, H. J. Zhang, D. H. Lu, X. Dai, Z. Fang, S.-C. Zhang, I. R. Fisher, Z. Hussain, and Z. X. Shen, Science **325**, 178 (2009).

[22] D. X. Qu, Y. S. Hor, J. Xiong, R. J. Cava, and N. P. Ong, Science **329**, 821 (2010).

[23] Tong Zhang, Jeonghoon Ha, Niv Levy, Young Kuk, and Joseph Stroscio, Phys. Rev. Lett. **111**, 056803 (2013).

[24] Bahadur Singh, Ashutosh Sharma, H. Lin, M. Z. Hasan, R. Prasad, and A. Bansil, Phys. Rev. B **86**, 115208 (2012).

[25] T. Sato, Kouji Segawa, K. Kosaka, S. Souma, K. Nakayama, K. Eto, T. Minami, Yoichi Ando, and T. Takahashi, Nat. Phys. **7**, 840 (2011).

[26] Y. Xu, I. Miotkowski, C. Liu, J. Tian, H. Nam, N. Alidoust, J. Hu, C.-K. Shih, M. Z. Hasan, and Y. P. Chen, Nat. Phys. **10**, 956 (2014).

[27] R. Dornhaus and G. Nimtz, *Narrow Gap Semiconductors*, in Springer Tracts in Modern Physics Vol. 98 (Springer, Heidelberg, 1983).

[28] D. A. Kozlov, Z. D. Kvon, E. B. Olshanetsky, N. N. Mikhailov, S. A. Dvoretsky, and D. Weiss, Phys. Rev. Lett. **112**, 196801 (2014).

[29] A. Kisiel, M. Podgórny, A. Rodzik, and W. Giriat, Phys. Status Solidi B **71**, 457 (1975).

[30] J. G. Analytis, R. D. McDonald, S. C. Riggs4, J.-H. Chu, G. S. Boebinger, and I. R. Fisher, Nat. Phys. **6**, 960 (2010).

[31] B. F. Gao, P. Gehring, M. Burghard, and K. Kern, Appl. Phys. Lett. **100**, 212402 (2012).

[32] J. Olea, G. Gonzalez-Daz, D. Pastor, I. Martil1, A. Mart, E. Antoln, and A. Luque, J. Appl. Phys. **109**, 063718 (2011).

[33] G. M. Gusev, Z. D. Kvon, E. B. Olshanetsky, A. D. Levin, Y. Krupko, J. C. Portal, N. N. Mikhailov, and S. A. Dvoretsky, Phys. Rev. B **89**, 125305 (2014).

[34] K. S. Novoselov, A. K. Geim, S. V. Morozov, D. Jiang, M. I. Katsnelson, I. V. Grigorieva, S. V. Dubonos, and A. A. Firsov, Nature (London) **438**, 197 (2005).

[35] Y. Zhang, Y. W. Tan, H. L. Stormer, and P. Kim, Nature (London) **438**, 201 (2005).

[36] Yia-Chung Chang, J. N. Schulman, G. Bastard, Y. Guldner, and M. Voos, Phys. Rev. B **31**, 2557 (1985).

[37] Jie Ren, Guang Bian, Li Fu, Chang Liu, Tao Wang, Gangqiang Zha, Wanqi Jie, Madhab Neupane, T. Miller, M. Z. Hasan, and T.-C. Chiang, Phys. Rev. B **90**, 205211 (2014).

[38] Christoph Brüne, Cornelius Thienel, Michael Stuiber, Jan Böttcher, Hartmut Buhmann, Elena G. Novik, Chao-Xing Liu, Ewelina M. Hankiewicz, and Laurens W. Molenkamp, Phys. Rev. X **4**, 041045 (2014).

[39] E. H. Hwang and S. Das Sarma, Phys. Rev. B **75**, 205418 (2007).

[40] Steffen Wiedmann, Andreas Jost, Cornelius Thienel, Christoph Brüne, Philipp Leubner, Hartmut Buhmann, Laurens W. Molenkamp, J. C. Maan, and Uli Zeitler, Phys. Rev. B **91**, 205311 (2015).